

# 1 Combined polarized Raman and atomic force microscopy: *In situ* study 2 of point defects and mechanical properties in individual ZnO nanobelts

3 Marcel Lucas,<sup>1</sup> Zhong Lin Wang,<sup>2</sup> and Elisa Riedo<sup>1,a)</sup>

4 <sup>1</sup>*School of Physics, Georgia Institute of Technology, Atlanta, Georgia 30332-0430, USA*

5 <sup>2</sup>*School of Materials Science and Engineering, Georgia Institute of Technology, Atlanta,*  
6 *Georgia 30332-0245, USA*

7 (Received 8 June 2009; accepted 23 June 2009; published online xx xx xxxx)

8 We present a method, polarized Raman (PR) spectroscopy combined with atomic Force microscopy  
9 (AFM), to characterize *in situ* and nondestructively the structure and the physical properties of  
10 individual nanostructures. PR-AFM applied to individual ZnO nanobelts reveals the interplay  
11 between growth direction, point defects, morphology, and mechanical properties of these  
12 nanostructures. In particular, we find that the presence of point defects can decrease the elastic  
13 modulus of the nanobelts by one order of magnitude. More generally, PR-AFM can be extended to  
14 different types of nanostructures, which can be in as-fabricated devices. © 2009 American Institute  
15 of Physics. [DOI: 10.1063/1.3177065]

17 Nanostructured materials, such as nanotubes, nanobelts  
18 (NBs), and thin films, have potential applications as elec-  
19 tronic components, catalysts, sensors, biomarkers, and en-  
20 ergy harvesters.<sup>1-5</sup> The growth direction of single-crystal  
21 nanostructures affects their mechanical,<sup>6-8</sup> optoelectronic,<sup>9</sup>  
22 transport,<sup>4</sup> catalytic,<sup>5</sup> and tribological properties.<sup>10</sup> Recently,  
23 ZnO nanostructures have attracted a considerable interest for  
24 their unique piezoelectric, optoelectronic, and field emission  
25 properties.<sup>1,2,11,12</sup> Numerous experimental and theoretical  
26 studies have been undertaken to understand the properties of  
27 ZnO nanowires and NBs,<sup>11,12</sup> but several questions remain  
28 open. For example, it is often assumed that oxygen vacancies  
29 are present in bulk ZnO, and that their presence reduces the  
30 mechanical performance of ZnO materials.<sup>13</sup> However, no  
31 direct observation has supported the idea that point defects  
32 affect the mechanical properties of individual nanostructures.

33 Only a few combinations of experimental techniques en-  
34 able the investigation of the mechanical properties, morphol-  
35 ogy, crystallographic structure/orientation and presence of  
36 defects in the same individual nanostructure, and they are  
37 rarely implemented due to technical challenges. Transmis-  
38 sion electron microscopy (TEM) can determine the crystal-  
39 lographic structure and morphology of nanomaterials that are  
40 thin enough for electrons to transmit through,<sup>4,14-17</sup> but suf-  
41 fers from some limitations. For example, characterization of  
42 point defects is rather challenging.<sup>14-17</sup> Also, the *in situ* TEM  
43 characterization of the mechanical and electronic properties  
44 of nanostructures is very challenging or impossible.<sup>15-17</sup>  
45 Alternatively, atomic force microscopy (AFM) is well  
46 suited for probing the morphology, mechanical, magnetic,  
47 and electronic properties of nanostructures from the  
48 micron scale down to the atomic scale.<sup>3,6,7,10</sup> In parallel,  
49 Raman spectroscopy is effective in the characterization of  
50 the structure, mechanical deformation, and thermal proper-  
51 ties of nanostructures,<sup>18,19</sup> as well as the identification of  
52 impurities.<sup>20</sup> Furthermore, polarized Raman (PR) spectro-  
53 scopy was recently used to characterize the crystal structure  
54 and growth direction of individual single-crystal  
55 nanowires.<sup>21</sup>

56 Here, an AFM is combined to a Raman microscope  
57 through an inverted optical microscope. The morphology and  
58 the mechanical properties of individual ZnO NBs are deter-  
59 mined by AFM, while polarized Raman spectroscopy is used  
60 to characterize *in situ* and nondestructively the growth direc-  
61 tion and randomly distributed defects in the same individual  
62 NBs. We find that the presence of point defects can decrease  
63 the elastic modulus of the NBs by almost one order of mag-  
64 nitude.

65 The ZnO NBs were prepared by physical vapor deposi-  
66 tion (PVD) without catalysts<sup>14</sup> and deposited on a glass  
67 cover slip. For the PR studies, the cover slip was glued to the  
68 bottom of a Petri dish, in which a hole was drilled to allow  
69 the laser beam to go through it. The round Petri dish was  
70 then placed on a sample plate below the AFM scanner, where  
71 it can be rotated by an angle  $\varphi$ , or clamped (see Fig. 1). The  
72 morphology and mechanical properties of the ZnO NBs were  
73 characterized with an Agilent PicoPlus AFM. The AFM was  
74 placed on top of an Olympus IX71 inverted optical micro-  
75 scope using a quickslide stage (Agilent). A silicon AFM  
76 probe (PointProbe NCHR from Nanoworld), with a normal  
77 cantilever spring constant of 26 N/m and a radius of about  
78 60 nm, was used to collect the AFM topography and  
79 modulated nanoindentation data. The elastic modulus of the  
80 NBs was measured using the modulated nanoindentation  
81 method<sup>22</sup> by applying normal displacement oscillations at the  
82 frequency of 994.8 Hz, at the amplitude of 1.2 Å, and by  
83 varying the normal load. PR spectra were recorded in the  
84 backscattering geometry using a laser spot small enough  
85 (diameter of 1–2  $\mu\text{m}$ ) to probe one single NB at a time. The  
86 incident polarization direction can be rotated continuously  
87 with a half-wave plate and the scattered light is analyzed  
88 along one of two perpendicular directions by a polarizer at  
89 the entrance of the spectrometer (Fig. 1). Series of PR spec-  
90 tra from the bulk ZnO crystals and the individual ZnO NBs  
91 were collected with varying sample orientation  $\varphi$  (the NBs  
92 are parallel to the incident polarization at  $\varphi=0$ ), in the co-  
93 (parallel incident and scattered analyzed polarizations) and  
94 cross-polarized (perpendicular incident and scattered ana-  
95 lyzed polarizations) configurations. For the ZnO NBs, addi-  
96 tional series of PR spectra were collected where the incident

<sup>a)</sup>Electronic mail: elisa.riedo@physics.gatech.edu.

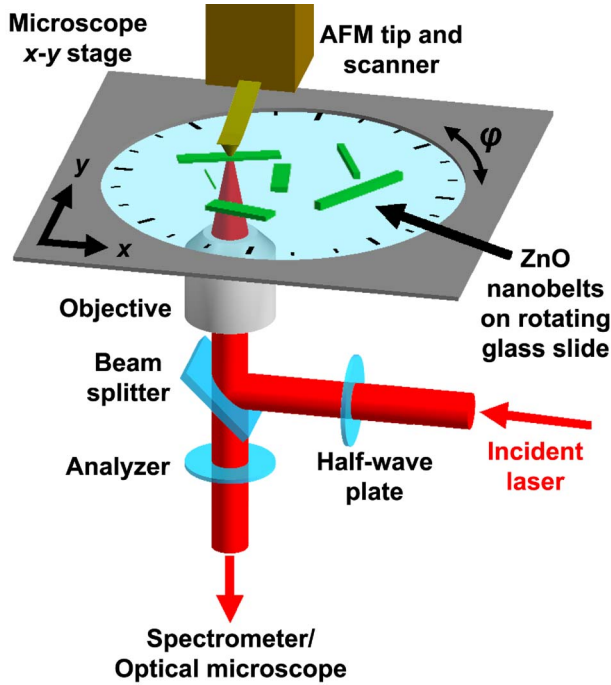


FIG. 1. (Color online) Schematic of the experimental setup, showing the path of the laser beam. The ZnO NBs are deposited on a glass slide, which is placed inside a rotating Petri dish.

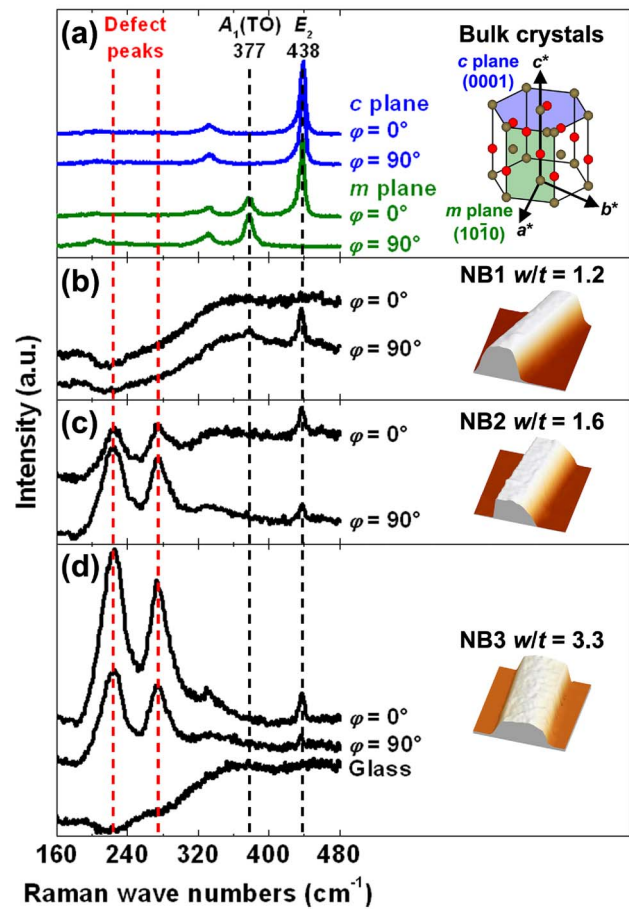


FIG. 2. (Color online) (a) PR spectra from the  $c$  and  $m$  planes of a ZnO crystal, shown in blue and green, respectively. The wurtzite structure (Zn atoms are brown, O atoms red) is also shown, where  $a^*$ ,  $b^*$ , and  $c^*$  are the reciprocal lattice vectors. [(b)–(d)] AFM images ( $3 \times 3 \mu\text{m}$ ) of three NBs labeled NB1, NB2, and NB3 and corresponding PR spectra. In (d) a PR spectrum of the glass substrate is shown at the bottom. All the PR spectra in (a)–(d) are collected in the copolarized configuration for  $\varphi=0$  and  $90^\circ$ . The spectra are offset vertically for clarity.

AQ:  
#3

97 polarization is rotated and the ZnO NB axis remained paral-  
98 lel or perpendicular to the analyzed scattered polarization  
99 (see supplementary information<sup>25</sup>). The exposure time for  
100 each Raman spectrum was 10 s for the bulk crystals and 20  
101 min for NBs. After each rotation of the NBs, the laser spot is  
102 recentered on the same NB and at the same location along  
103 the NB.

104 Prior to the PR characterization of ZnO NBs, PR data  
105 were collected on the  $c$ -plane and  $m$ -plane of bulk ZnO  
106 crystals [Fig. 2(a)]. In ambient conditions, ZnO has a  
107 wurtzite structure (space group  $C_{6v}^4$ ). Group theory predicts  
108 four Raman-active modes: one  $A_1$ , one  $E_1$ , and two  $E_2$   
109 modes.<sup>11,20,23</sup> The polar  $A_1$  and  $E_1$  modes split into transverse  
110 (TO) and longitudinal optical branches. On the  $c$ -plane  
111 (0001)-oriented sample, only the  $E_2$  modes, at 99 (not  
112 shown) and  $438 \text{ cm}^{-1}$ , are observed, and their intensity is  
113 independent of the sample orientation  $\varphi$  [Fig. 2(a)]. On the  
114  $m$ -plane (10 $\bar{1}$ 0)-oriented sample, the  $E_2$ ,  $E_1$  (TO), and  $A_1$   
115 (TO) modes are observed at 99, 438, 409, and  $377 \text{ cm}^{-1}$ ,  
116 respectively [Fig. 2(a)], and their intensity depends on  $\varphi$ .  
117 Peaks at  $203$  and  $331 \text{ cm}^{-1}$  in both crystals are assigned to  
118 multiple phonon scattering processes. The intensity, center,  
119 and width of the peaks at  $438$ ,  $409$ , and  $377 \text{ cm}^{-1}$  were  
120 obtained by fitting the experimental PR spectra with Lorent-  
121 zian lines (see supplementary information<sup>25</sup>). The successful  
122 fits of the angular dependencies by using the group theory  
123 and crystal symmetry<sup>23</sup> indicate that PR data can be used to  
124 characterize the growth direction of ZnO NBs. It is noted  
125 that the ZnO NBs studied here have dimensions over  $300$   
126 nm, so the determination of the growth direction is not ex-  
127 pected to be affected by any enhancement of the polarized  
128 Raman signal due to their high aspect ratio.<sup>24</sup>

129 AFM images and PR data of three individual ZnO NBs  
130 are presented in Figs. 2(b)–2(d). These NBs, labeled NB1,  
131 NB2, and NB3, have different dimensions and properties as

summarized in Table I. A comparison of the PR spectra in 132  
Figs. 2(a)–2(d) reveals differences between bulk ZnO and 133  
individual NBs. First, the glass cover slip gives rise to a 134  
weak broadband centered around  $350 \text{ cm}^{-1}$  on the Raman 135  
spectra of the NBs [see bottom of Fig. 2(d)]. Second, there 136  
are additional Raman bands around  $224$  and  $275 \text{ cm}^{-1}$  for 137  
NB2 and NB3. These bands are observed in doped or ion- 138  
implanted ZnO crystals.<sup>11,20</sup> Their appearance is explained 139  
by the disorder in the crystal lattice due to randomly distrib- 140  
uted point defects, such as oxygen vacancies or impurities. 141  
The defect peaks area increases in the order  $\text{NB1} < \text{NB2}$  142  
 $< \text{NB3}$ . Since the laser spot diameter is larger than the width 143  
of all three NBs, but smaller than their length,  $L$ , the NB 144  
volume probed by the laser beam is approximated by the 145  
product of the width,  $w$ , with the thickness,  $t$ . The volume 146

TABLE I. Summary of the PR-AFM results for NB1, NB2, and NB3.

|     | $w$<br>(nm) | $t$<br>(nm) | $L$<br>( $\mu\text{m}$ ) | $\theta$<br>( $^\circ$ ) | $E$<br>(GPa) | Defects    |     |
|-----|-------------|-------------|--------------------------|--------------------------|--------------|------------|-----|
| NB1 | 1080        | 875         | 1.2                      | 40                       | $28 \pm 15$  | $62 \pm 5$ | No  |
| NB2 | 1150        | 710         | 1.6                      | 49                       | $72 \pm 15$  | $38 \pm 5$ | Yes |
| NB3 | 1510        | 455         | 3.3                      | 59                       | $66 \pm 15$  | $17 \pm 5$ | Yes |

147 probed decreases in the order  $NB1(w \times t = 9.45 \times 10^3 \text{ nm}^2)$   
 148  $> NB2(8.17 \times 10^3 \text{ nm}^2) > NB3(6.87 \times 10^3 \text{ nm}^2)$ . This indi-  
 149 cates that the density of point defects is highest in NB3, and  
 150 increases with the width to thickness ratio,  $w/t$ , in the order  
 151  $NB1 < NB2 < NB3$ .

152 The PR intensity variations of the  $438 \text{ cm}^{-1}$  peak as a  
 153 function of  $\varphi$  in the various polarization configurations were  
 154 fitted by using group theory and crystal symmetry to deter-  
 155 mine the angle  $\theta$  between the NB long axis (or growth di-  
 156 rection) and the  $c$ -axis ([0001] axis) of the constituting ZnO  
 157 wurtzite structure<sup>21,23</sup> (see supplementary information<sup>25</sup>). In-  
 158 tensity variations of the  $377 \text{ cm}^{-1}$  peak, when present, are  
 159 used to confirm the obtained values of  $\theta$ . The results are  
 160 shown in Table I and indicate that growth directions other  
 161 than the most commonly observed  $c$ -axis are possible, par-  
 162 ticularly when point defects are present.

163 Finally, the elastic properties of NB1, NB2, and NB3 are  
 164 characterized by AFM using the modulated nanoindentation  
 165 method.<sup>6,7,22</sup> In a previous study, the elastic modulus of ZnO  
 166 NBs was found to decrease with increasing  $w/t$  and this  $w/t$   
 167 dependence was attributed to the presence of planar defects  
 168 in NBs with high  $w/t$ .<sup>6,7</sup> By using PR-AFM, we can study  
 169 the role of randomly distributed defects, morphology, and  
 170 growth direction on the elastic properties in the same indi-  
 171 vidual ZnO NB. The measured elastic moduli,  $E$ , are 62 GPa  
 172 for NB1, 38 GPa for NB2, and 17 GPa for NB3. These  
 173 PR-AFM results confirm the  $w/t$  dependence of the elastic  
 174 modulus in ZnO NBs, but more importantly they reveal that  
 175 the elastic modulus of ZnO NBs can significantly decrease,  
 176 down by almost one order of magnitude, with the presence of  
 177 randomly distributed point defects.

178 In summary, a new approach combining polarized  
 179 Raman spectroscopy and AFM reveals the strong influence  
 180 of point defects on the elastic properties of ZnO NBs and  
 181 their morphology. Based on a scanning probe, PR-AFM pro-  
 182 vides an *in situ* and nondestructive tool for the complete  
 183 characterization of the crystal structure and the physical  
 184 properties of individual nanostructures that can be in as-  
 185 fabricated nanodevices.

The authors acknowledge the financial support from 186  
 the Department of Energy under Grant No. DE-FG02- 187  
 06ER46293. 188

- <sup>1</sup>Y. Qin, X. Wang, and Z. L. Wang, *Nature (London)* **451**, 809 (2008). 189  
<sup>2</sup>X. Wang, J. Song, J. Liu, and Z. L. Wang, *Science* **316**, 102 (2007). 190  
<sup>3</sup>D. J. Müller and Y. F. Dufrène, *Nat. Nanotechnol.* **3**, 261 (2008). 191  
<sup>4</sup>H. Peng, C. Xie, D. T. Schoen, and Y. Cui, *Nano Lett.* **8**, 1511 (2008). 192  
<sup>5</sup>U. Diebold, *Surf. Sci. Rep.* **48**, 53 (2003). 193  
<sup>6</sup>M. Lucas, W. J. Mai, R. Yang, Z. L. Wang, and E. Riedo, *Nano Lett.* **7**, 1314 (2007). 194  
<sup>7</sup>M. Lucas, W. J. Mai, R. Yang, Z. L. Wang, and E. Riedo, *Philos. Mag.* **87**, 2135 (2007). 195  
<sup>8</sup>M. D. Uchic, D. M. Dimiduk, J. N. Florando, and W. D. Nix, *Science* **305**, 986 (2004). 196  
<sup>9</sup>D.-S. Yang, C. Lao, and A. H. Zewail, *Science* **321**, 1660 (2008). 197  
<sup>10</sup>M. Dienwiebel, G. S. Verhoeven, N. Pradeep, J. W. M. Frenken, J. A. Heimberg, and H. W. Zandbergen, *Phys. Rev. Lett.* **92**, 126101 (2004). 198  
<sup>11</sup>Ü. Özgür, Ya. I. Alivov, C. Liu, A. Teke, M. A. Reshchikov, S. Doğan, V. Avrutin, S.-J. Cho, and H. Morkoç, *J. Appl. Phys.* **98**, 041301 (2005). 199  
<sup>12</sup>Z. L. Wang, *J. Phys.: Condens. Matter* **16**, R829 (2004). 200  
<sup>13</sup>G. R. Li, T. Hu, G. L. Pan, T. Y. Yan, X. P. Gao, and H. Y. Zhu, *J. Phys. Chem. C* **112**, 11859 (2008). 201  
<sup>14</sup>Z. W. Pan, Z. R. Dai, and Z. L. Wang, *Science* **291**, 1947 (2001). 202  
<sup>15</sup>P. Poncharal, Z. L. Wang, D. Ugarte, and W. A. De Heer, *Science* **283**, 1513 (1999). 203  
<sup>16</sup>A. M. Minor, J. W. Morris, and E. A. Stach, *Appl. Phys. Lett.* **79**, 1625 (2001). 204  
<sup>17</sup>B. Varghese, Y. Zhang, L. Dai, V. B. C. Tan, C. T. Lim, and C.-H. Sow, *Nano Lett.* **8**, 3226 (2008). 205  
<sup>18</sup>M. Lucas and R. J. Young, *Phys. Rev. B* **69**, 085405 (2004). 206  
<sup>19</sup>I. Calizo, A. A. Balandin, W. Bao, F. Miao, and C. N. Lau, *Nano Lett.* **7**, 2645 (2007). 207  
<sup>20</sup>H. Zhong, J. Wang, X. Chen, Z. Li, W. Xu, and W. Lu, *J. Appl. Phys.* **99**, 103905 (2006). 208  
<sup>21</sup>T. Livneh, J. Zhang, G. Cheng, and M. Moskovits, *Phys. Rev. B* **74**, 035320 (2006). 209  
<sup>22</sup>I. Palaci, S. Fedrigo, H. Brune, C. Klinke, M. Chen, and E. Riedo, *Phys. Rev. Lett.* **94**, 175502 (2005). 210  
<sup>23</sup>C. A. Arguello, D. L. Rousseau, and S. P. S. Porto, *Phys. Rev.* **181**, 1351 (1969). 211  
<sup>24</sup>H. M. Fan, X. F. Fan, Z. H. Ni, Z. X. Shen, Y. P. Feng, and B. S. Zou, *J. Phys. Chem. C* **112**, 1865 (2008). 212  
<sup>25</sup>See EPAPS supplementary material at <http://dx.doi.org/10.1063/1.3177065> for ■. 213

AQ: 215  
 #1 216  
 217  
 218  
 219  
 220  
 221  
 222  
 223  
 224  
 225  
 226  
 227  
 228  
 229 AQ:  
 #2

**AUTHOR QUERIES — 074928APL**

- #1 Au: Please check accuracy of year in Ref. 17
- #2 Au: Please supply brief description of supplementary material in Ref. 25
- #3 Au: Although a caption makes reference to color online, figures will appear black and white in print. Please make sure the caption makes sense to print reader